Appl. Phys. A (2016) 122:466
DOI 10.1007/s00339-016-9939-4

Applied Physics A
Materials Science & Processing

Formation of copper tin sulfide films by pulsed laser deposition at 248 and 355 nm

Rebecca Bolt Ettlinger[1] · Andrea Crovetto[2] · Stela Canulescu[1] · Andrea Cazzaniga[1] · Lasse Ravnkilde[2] · Tomas Youngman[2] · Ole Hansen[2] · Nini Pryds[3] · Jørgen Schou[1]

Received: 16 October 2015 / Accepted: 23 February 2016 / Published online: 29 March 2016

Abstract The influence of the laser wavelength on the deposition of copper tin sulfide (CTS) and SnS-rich CTS with a 248-nm KrF excimer laser (pulse length $\tau = 20$ ns) and a 355-nm frequency-tripled Nd:YAG laser ($\tau = 6$ ns) was investigated. A comparative study of the two UV wavelengths shows that the CTS film growth rate per pulse was three to four times lower with the 248-nm laser than the 355-nm laser. SnS-rich CTS is more efficiently ablated than pure CTS. Films deposited at high fluence have submicron and micrometer size droplets, and the size and area density of the droplets do not vary significantly from 248 to 355 nm deposition. Irradiation at low fluence resulted in a non-stoichiometric material transfer with significant Cu deficiency in the as-deposited films. We discuss the transition from a non-stoichiometric material transfer at low fluence to a nearly stoichiometric ablation at high fluence based on a transition from a dominant evaporation regime to an ablation regime.

1 Introduction

Research in thin-film solar cells based on p-type semiconductors has mainly been focused on $Cu(In,Ga)(S,Se)_2$ (CIGS) and CdTe. However, due to the limited availability of elements such as In and Te and the toxicity of Cd, alternative absorbers such as Cu_2ZnSnS_4 (CZTS) are being investigated [1], and recently, a thin-film solar cell based on a CZTS absorber layer has reached an efficiency of 8.8 % [2]. Other p-type semiconductors with fewer elements are also available, including members of the ternary Cu–Sn–S system [3]. Among the Cu–Sn–S compounds, Cu_2SnS_3 (CTS) has been suggested as potential solar cell absorber because it has an absorption coefficient comparable to CZTS and a band gap of 0.9–1.35 eV depending on the crystal structure [4–6]. The highest efficiency of CTS solar cells of 4.65 % was achieved by thermal evaporation [7]. CTS thin films have also, more recently, been fabricated by pulsed laser deposition (PLD) [8]. Vanalakar

✉ Rebecca Bolt Ettlinger
reet@fotonik.dtu.dk

Andrea Crovetto
ancro@nanotech.dtu.dk

Stela Canulescu
stec@fotonik.dtu.dk

Andrea Cazzaniga
andcan@fotonik.dtu.dk

Lasse Ravnkilde
s122729@student.dtu.dk

Tomas Youngman
s123603@student.dtu.dk

Ole Hansen
ole.hansen@nanotech.dtu.dk

Nini Pryds
nipr@dtu.dk

Jørgen Schou
josc@fotonik.dtu.dk

[1] DTU Fotonik, Technical University of Denmark, Frederiksborgvej 399, 4000 Roskilde, Denmark

[2] DTU Nanotech, Technical University of Denmark, 2800 Kgs. Lyngby, Denmark

[3] DTU Energy, Technical University of Denmark, 4000 Roskilde, Denmark

et al. [9] have reported on the first CTS solar cell prepared by pulsed laser deposition with an efficiency of 0.82 %.

PLD is a suitable technique for the deposition of films with complex structures [10]. The presence of droplets (in some papers called particulates) in the growing films is a well-known problem, which can be addressed in a number of ways [11]. Particularly, droplets up to 1 micron in diameter or larger were observed in the films of CTS deposited by PLD [8, 9]. The influence of droplets on the overall efficiency of the solar cell is not well understood, but it is clear that it can be detrimental for the cell performance for the following reasons: (1) The droplet size can be larger than the overall thickness of the absorber layer, resulting in a rough interface and possible shunt paths between the CTS film and the subsequent solar cell layers [12], and (2) the droplets can have a different composition than the matrix of the CTS film [13, 14], resulting in non-homogeneity in composition and therefore different charge carrier transport properties.

Round droplets of micrometer or submicrometer size result from solidification of molten droplets ejected from the target by laser-induced recoil pressure or subsurface boiling [11]. A common approach to minimize droplets is to reduce the irradiation wavelength, as previously reported for Si [15], ZnO [16], and $YBa_2Cu_3O_{7-x}$ (YBCO) [17, 18] with comparisons of PLD using IR, visible, and UV laser wavelengths. Several mechanisms have been proposed to explain the better morphology of films deposited at UV wavelengths. First, the absorption depth (α^{-1}) in the material is usually short at UV wavelengths, resulting in a thin layer being ablated and thus formation of a hot plasma plume [17]. Second, if the absorption does not vary significantly with irradiation wavelength, droplet minimization may result from absorption of UV light by the droplets in the near-surface region, resulting in fragmentation down to a very small size. The second mechanism may be more dominant when comparing the morphology of films deposited at different UV wavelengths [17].

Apart from changing the laser wavelength, it is also known that a reduction in fluence can lead to a reduction in droplet area density and size [19]. A reduction in droplet density and size with a reduction of the fluence from 1.5 to 0.7 J/cm^2 has been seen in PLD of CZTS with a 248-nm laser by Moriya et al. [20] and with a reduction in fluence from 4 to 0.5 J/cm^2 on CZTS using a 355-nm laser by Sulaiman et al. [13]. Pawar et al. [21] also observed smaller and fewer droplets at 1 J/cm^2 than at 1.5 and 2 J/cm^2 using a 248-nm laser with CZTS. Similarly, Ujimoto et al. [22] observed a reduction in droplet density from 1.5 to 0.5 J/cm^2 using a 193-nm excimer laser to deposit $BiFeO_3$, while noting that in their case droplets could not be completely avoided simply by decreasing laser fluence.

The aim of this paper is to examine the influence of two different UV laser wavelengths on the deposition rate and the size, density, and composition of the droplets in films deposited by PLD from targets of CTS and SnS-enriched CTS. The SnS-rich composition was chosen for comparison because deficiency of Sn and S had previously been observed in CTS films deposited with 355-nm laser irradiation [8].

2 Materials and methods

2.1 Pulsed laser deposition

Pulsed laser deposition was carried out using a Nd:YAG laser operating at 355 nm (third harmonic) with a pulse duration of 5–7 ns and a KrF excimer laser operating at 248 nm with a pulse duration of 20 ns (see Fig. 1; Table 1). The depositions were made in vacuum at a pressure of 1–5 $\times$ 10^{-6} mbar. The target was placed at an angle of 45° with respect to the incoming laser beam, and the beam was rastered across the target. The substrate material was Mo-coated soda-lime glass, which is typically used for CTS solar cell preparation. The fluence was varied from 0.2 to 2.3 J/cm^2 and was calculated based on a measurement of the spot size on a Cu foil. The substrate–target distance was 4–4.5 cm due to constraints in the setups for ensuring similar deposition conditions. Films made using the 355 nm laser with target–substrate distances ranging from 4 cm to 7.5 cm were similar in composition and droplet density (not shown), as expected for depositions made in vacuum [19].

Single samples were made at different fluence values and spot sizes. The representativeness of the single samples was verified by repeated depositions of some of the films under identical circumstances. With the 355-nm laser and

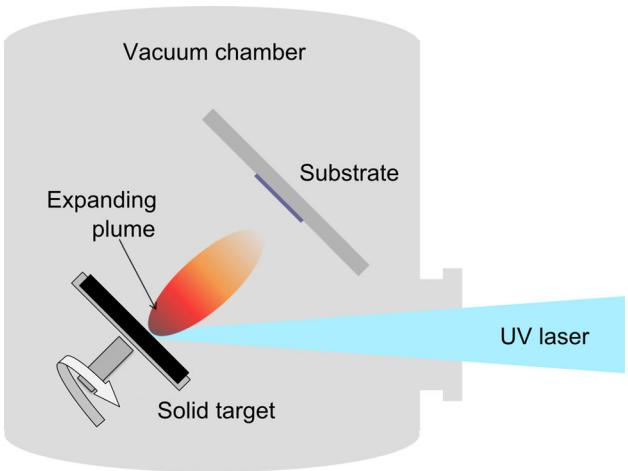

Fig. 1 Setup. See Table 1 for comparison of the 248 and 355 nm setups

Table 1 Laser and setup comparison

Wavelength (λ)	248 nm	355 nm
Laser type	KrF excimer	Nd:YAG solid-state
Pulse width (ns)	20	5–7
Frequency (Hz)	10	10
Target–substrate distance (cm)	4	4–4.5[a]
Spot size (mm^2)	2.2 ± 0.1[a]	2.2 ± 0.1[a]
Fluence range (J/cm^2)	0.2–2.1	0.2–2.4
Duration of deposition (min)	45–94	20–180

[a] All measurements with the quartz crystal microbalance were made with a target–substrate distance of 4 cm and a spot size of 2.2 ± 0.1 mm^2. The films at low fluence (0.2–0.5 J/cm^2) were made with a larger spot size (up to 5 ± 0.2 mm^2) in order to make a relatively thick film within a reasonable amount of time

the SnS-rich CTS target, nine films were made under exactly the same circumstances, confirming that the deposition rate, droplet density (appearance in SEM), and composition were reproducible. With the non-SnS-enriched CTS target, films made at 1.6 J/cm^2 were reproduced with both lasers and it was confirmed that samples produced under the same circumstances were similar regarding thickness, droplet density, and composition.

The number of pulses at the two different wavelengths was adjusted to deposit films sufficiently thick for reliable energy-dispersive X-ray spectroscopy (EDX) at most fluences. According to the model CASINO [23], 99 % of the EDX signal for CTS derives from below 900 nm thickness and 90 % from below 750 nm, assuming a smooth surface and a bulk density of 5.02 g/cm^3 for Cu_2SnS_3 [24].

Multicomponent targets of CTS and SnS-rich CTS were purchased from PVD products. The targets named "CTS" in the present work had a Cu:Sn:S ratio of about 2:1:2.5 (measured by EDX; see Table 2), while the one called "SnS-rich CTS" had a Cu:Sn:S ratio of about 1:2:3. The targets consisted of multiple crystalline phases identified by XRD including Cu_2SnS_3 (tetragonal, JCPDS 89-4714), SnS (cubic, JCPDS 89-2755, and orthorhombic, JCPDS 75-1803), CuS (cubic, JCPDS 78-877), and Cu_2S (cubic, JCPDS 53-522). EDX mapping of the targets showed regions of hundreds of micrometers in diameter with either Cu-rich composition, Sn-rich composition, or a mixture of different phases.

2.2 Characterization

The deposition rates were measured with quartz crystal microbalances (QCM, Colnatec, Inc) and converted to film thickness, assuming a bulk density of 5.02 g/cm^3 for both Cu_2SnS_3 and SnS-rich CTS (the bulk density of SnS of 5.08 g/cm^3 is similar to that of CTS) [24, 25]. The targets were pre-ablated by 15.000–18.000 pulses before the measurement of the deposition rate in order to ensure a stable deposition. As shown in Table 1, the ablation parameters were similar for the comparison of the deposition rate between the different wavelengths. The deposition rates measured by QCM were systematically larger (by about 20–30 %) than the deposition rates determined from thickness measurements of films made at different fluence values (data not shown). This was most likely due to the measurement method: In SEM, the measurement excluded droplets sticking up above the film surface, while Dektak measurements are not highly accurate for surfaces with a high density of micrometer-scale droplets.

X-ray diffraction (XRD) measurements were carried out with a Bruker D8 diffractometer in Bragg–Brentano configuration using Cu K_α and Cu K_β radiation. The diffraction pattern of the as-deposited films was measured using a step size of 0.03° and a rate of 0.33 step/s.

Scanning electron microscopy was performed at 5–15 kV using the in-lens and secondary electron detectors of two SEMs equipped with field emission guns (FE-SEM, Supra 60VP and Supra 35, Zeiss). The droplet size distributions were determined by processing SEM images of 20 × 30 μm size with image analysis software (ImageJ). The droplets were discriminated from the homogeneous

Table 2 Composition of the CTS target and selected films deposited at room temperature

	Fluence (J/cm^2)	Spot size (mm^2)	Thickness (nm)	Cu (%)	Sn (%)	S (%)	Cu/Sn
CTS target	–	–	–	38.6 ± 1.0	17.1 ± 1.0	44.4 ± 0.3	2.3 ± 0.5
355-nm laser	1.6	2.5	1500	43.3 ± 0.4	18.7 ± 0.5	38.1 ± 0.1	2.3 ± 0.1
	0.5	5	1000	28.8 ± 0.5	25.8 ± 0.5	45.5 ± 0.1	1.1 ± 0.1
	0.2	3.3	1200	27.4 ± 0.7	25.3 ± 0.3	47.3 ± 0.5	1.1 ± 0.1
248-nm laser	1.6	2.2	850–900	38.9 ± 0.6	19.3 ± 0.2	41.8 ± 0.6	2.0 ± 0.1
	0.5	5	800	11.1 ± 1	29.2 ± 2.1	59.8 ± 2.3	0.4 ± 0.1
	0.2	4	450	*ND*	*ND*	*ND*	*ND*

Uncertainties are the standard error of repeated measurements with the same instrument. The standard error on the Cu/Sn ratio is calculated, assuming that the Cu and Sn content are fully anti-correlated. All the film measurements in this table were made with the Bruker detector

film using a semiautomatic procedure with the signal intensity contrast as selection criterion and the area of each droplet was calculated automatically. Energy-dispersive X-ray spectroscopy (EDX) was performed at 15 kV in a Hitachi TM3000 tabletop SEM using a built-in Bruker detector with Quantax 70 software that performed mapping and quantification of the element ratios with Cu K-lines. Additional EDX measurements were performed in the Supra 60VP SEM with a silicon drift detector (X-Man^N 50, Oxford Instruments), which allowed measurement on specific areas identified in SEM images of the films including individual droplets. From the Supra/X-Man^N 50 data, element ratios were calculated by Oxford Instrument's Aztec software using the Cu K-lines and deconvoluting any Mo contribution to the S peak.

3 Results

3.1 Deposition rates

The deposition rate of CTS and SnS-rich CTS as a function of laser fluence is shown in Fig. 2. At any given fluence, the deposition rate of CTS and SnS-rich CTS at 355 nm is three to four times higher than at 248 nm.

Two main factors may explain the difference in deposition rate between the two lasers. Firstly, the effective intensity at 248 nm (1.2×10^8 W/cm^2) was about three times lower than at 355 nm (3.8×10^8 W/cm^2) due to the longer pulse duration at 248 nm. Secondly, the photon energy of 5 eV (corresponding to 248 nm) and 3.5 eV (corresponding to 355 nm) is much larger that the band gap energy of the constituent phases of the target, which was mainly composed of SnS, CuS, Cu_2S, and tetragonal-phase Cu_2SnS_3 (see Sect. 2.1) [4, 26, 27]. However, it is possible that the absorption coefficient of the individual phases varies from 248 to 355 nm even though the photon energies are greater than the band gap energy. For example, for a mixture of the two related phases, cubic-phase and monoclinic-phase Cu_2SnS_3, the absorption coefficient was found to vary by a factor 3 from 1.6×10^5 cm^{-1} at 3.5 eV to 4.3×10^5 cm^{-1} at 5 eV [28]. For SnS, the absorption coefficient varies less between the two wavelengths (both approx. 1×10^6 cm^{-1} as estimated from plots of the dielectric functions) [29]. The variation in the absorption coefficient means that the light penetration depth may vary from phase to phase in the target. Overall, the lower deposition yield at 248 nm compared to 355 nm probably may be attributed to the lower laser intensity, possibly in combination with a smaller light penetration depth in some of the phases in the target.

Figure 2 furthermore shows that the deposition of SnS-rich CTS (Cu:Sn:S 1:2:3) was faster than the deposition of CTS (Cu:Sn:S 2:1:2.5), independent of the irradiation wavelength. This is expected since both S and SnS have a higher vapor pressure than the copper-containing phases in the target [30, 31]. An increase in the concentration of high vapor pressure components in the target results in a higher ablation yield [10, 11].

3.2 Droplets

SEM images of several CTS and SnS-rich CTS films deposited at a laser fluence of 0.2–1.8 J/cm^2 are shown in Fig. 3a–f. The surface of the films is covered with large circular droplets ranging from tens of nanometers to

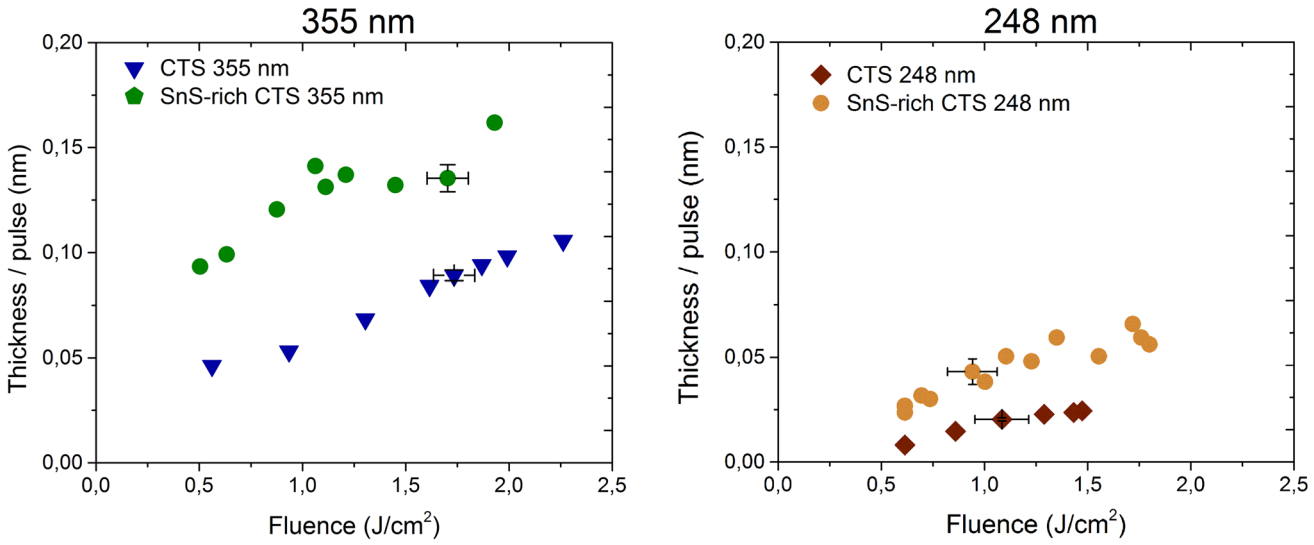

Fig. 2 Deposition rates of CTS and SnS-rich CTS at 355 nm (Nd:YAG laser, $\tau = 6$ ns) and 248 nm (KrF laser, $\tau = 20$ ns). The estimated error is similar for all the measurements, increasing proportionally with the fluence. Due to constraints in the 248 nm setup, it was not possible to measure the deposition rate at higher fluence without changing the spot size

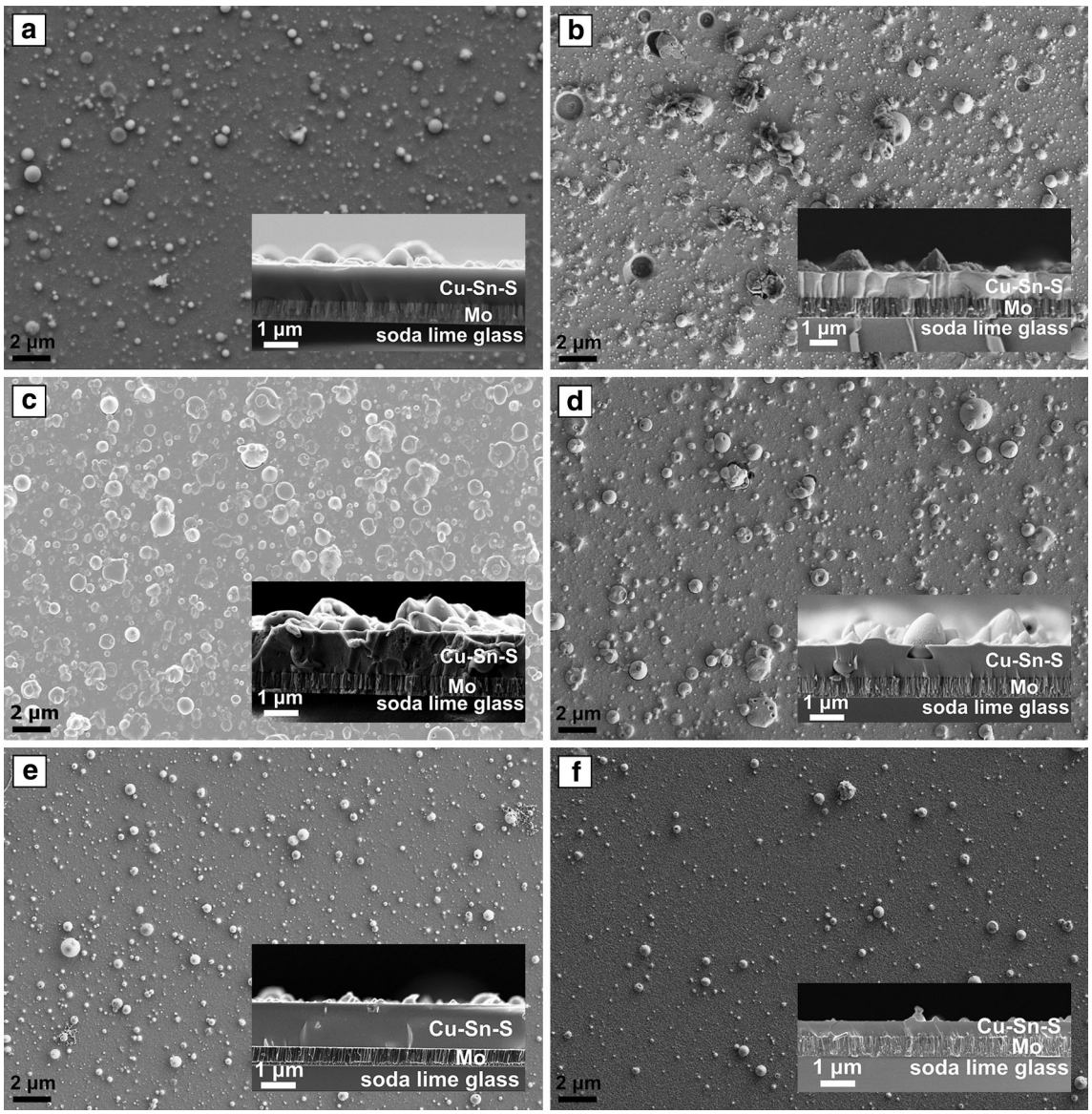

Fig. 3 SEM images (*top* and *side view*) of as-deposited films on Mo-coated soda-lime glass made at room temperature with 355 nm (**a**, **c**, **e**) and 248 nm (**b**, **d**, **f**) laser pulses. **a** 355 nm SnS-rich CTS 1.4 J/cm^2, **b** 248 nm SnS-rich CTS 1.8 J/cm^2, **c** 355 nm CTS 1.6 J/cm^2, **d** 248 nm CTS 1.6 J/cm^2, **e** 355 nm CTS 0.2 J/cm^2, **f** 248 nm CTS 0.2 J/cm^2 (note that this film was not used for EDX as it was too thin). While the 355-nm film shown in (**a**) was made at 1.4 J/cm^2, this film was highly similar to a series of films made at 2.3 J/cm^2 by the same laser. Image (**c**) was taken with the backscattered electron detector, while the others were taken with the more surface-sensitive secondary electron detectors

several microns in diameter. Our findings indicate that at a given fluence, the surface morphology of the as-deposited CTS films does not vary significantly from 355 to 248 nm. On the other hand, a decrease in the laser fluence to 0.2 J/cm^2 results in a decrease in the size and density of the droplets at both wavelengths (Fig. 3e–f).

The size distribution of the droplets extracted from SEM images in Fig. 3c–f is shown in Fig. 4. Note that we could not accurately identify small (<200 nm) particulates nor overlapping droplets by this method. The incidence of large droplets is also determined with a considerable uncertainty in the histograms as they were relatively rare. Nonetheless, Fig. 4 shows that there is no reduction in droplet area density for the 248-nm laser compared to the 355-nm laser. At high laser fluence, the distribution profile is broad, while at low fluence, the average size of the droplets decreases. The data suggest that the size and density of the droplets are strongly dependent on the laser energy and, for a given fluence, less dependent on the UV irradiation wavelength. This will be discussed in Sect. 4.

No diffraction peaks were observed beside Mo and MoO_x in X-ray diffractograms of the as-deposited films,

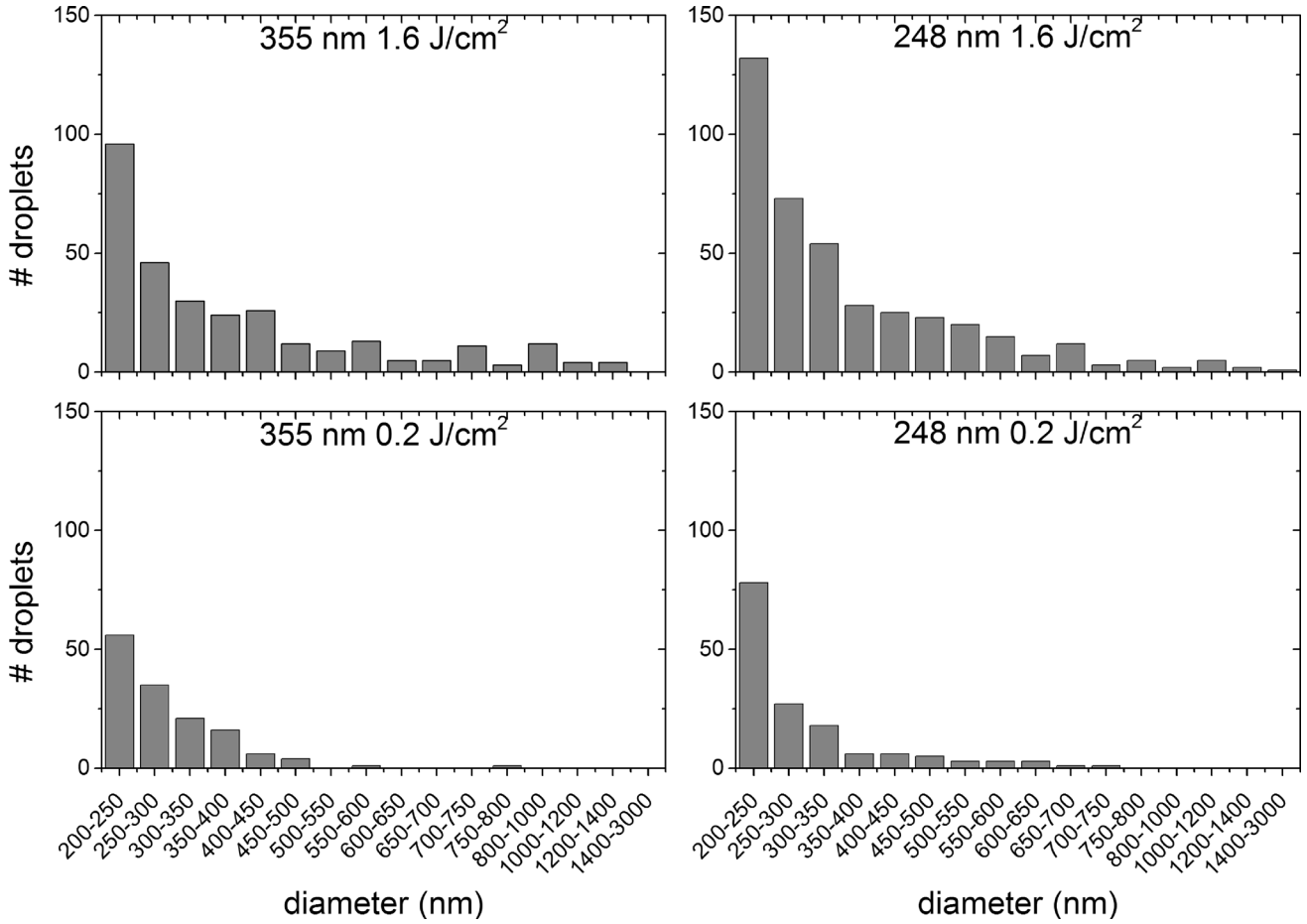

Fig. 4 Distribution of droplet size at 0.2 and 1.6 J/cm^2 with the 355- and 248-nm laser in a film made from the non-SnS-enriched target. Smaller droplets were present but could not be accurately quantified with the image processing software. Large droplets were rare and are therefore not accurately portrayed in the histograms

indicating that the films were mostly amorphous (X-ray data not shown).

3.3 Composition

Sulfur content The CTS films deposited at high fluence (1.5–1.6 J/cm^2) show S deficiency, and the deficiency appears to be larger at 355 nm than at 248 nm (Table 2). In contrast, the S content increased markedly in the films made at low fluence (0.5 J/cm^2 with the 355 nm and 0.2 J/cm^2 with the 248-nm laser). Thus, the S content increased from S/(Cu + Sn) = 0.8 ± 0.2 in the target to S/(Cu + Sn) = 1.5 ± 0.6 in the film made at 0.5 J/cm^2 by the 248-nm laser.

Metal content The Cu/Sn ratio of the target is maintained within the error bar in the CTS films made at 1.6 J/cm^2 by the 355-nm laser (Table 2). In comparison, the CTS film deposited at 248 nm at a similar fluence has a somewhat lower Cu concentration, though still within the error bar. The low-fluence depositions resulted in CTS films with a significant Cu deficiency at both wavelengths. The Cu/Sn ratio varies from 1.1 ± 0.1 for films made at 0.2–0.5 J/cm^2 at 355 nm to only 0.4 ± 0.1 for a film made at 0.5 J/cm^2 at 248 nm. These values should be compared with the Cu/Sn ratio in the target of 2.3 ± 0.5. As a general trend, we observe that as the incident laser energy is reduced, incongruent evaporation becomes dominant, and the Cu content in the as-deposited films decreases progressively (see Sect. 4). We have previously reported a similar but less dramatic increase in the S and Sn content of films made at low fluence with the 355-nm laser [8].

Composition of SnS-rich films The composition of the SnS-rich films does not vary much for films made at fluences between 0.7 and 2.3 J/cm^2 with the 355-nm laser or for films made at 1–1.8 J/cm^2 for the 248-nm laser (data not shown). In general, the films appear S- and Sn-poor compared to the target, but highly Sn-rich (Cu/Sn ~0.6) as well as somewhat S-poor compared to the desired stoichiometry of Cu_2SnS_3.

Composition of droplets The chemical composition versus the diameter of the droplets of the CTS films deposited at 1.6 J/cm^2 at 248 nm is shown in Fig. 5. EDX measurements

were carried out on a random selection of individual droplets with an average diameter larger than 1 μm. Figure 5 shows a significant deficiency of S and Sn and, consequently, enrichment of Cu in the Cu–Sn–S droplets. Despite the scattering of the data due to the relatively high uncertainty of the EDX analysis, we note that the deficiency of S and Sn increases as the droplet size decreases. The underlying film denoted by the "matrix" in Fig. 5 shows enrichment in the Sn content relative to the average target composition, which may derive from Sn loss from the droplets or from more efficient ablation of the Sn-rich phases in the target compared to the Cu-rich phases. The underlying film matrix is still slightly S deficient relative to the target, suggesting that sulfur losses occur both by evaporation from the film and by sulfur-deficient droplet solidification into the film.

It should be noted that the spot size was increased from 2.2 to 5 mm^2 in order to deposit films at low fluence due to the low deposition rate. The change in spot size may have had some influence on the off-axis composition, as the ablation plume becomes more forward-directed when the spot size is increased. However, we have in the present work considered the on-axis composition.

4 Discussion

Our ablation studies of CTS and SnS-rich CTS films indicate that the number of droplets is significantly reduced at lower laser fluence, while the irradiation wavelength does not significantly influence the surface morphology of the as-deposited CTS films. We observe a reduction in the average size of the droplets at low laser fluence accompanied by a change to non-stoichiometric material transfer with an increase in the S and Sn content. This trade-off

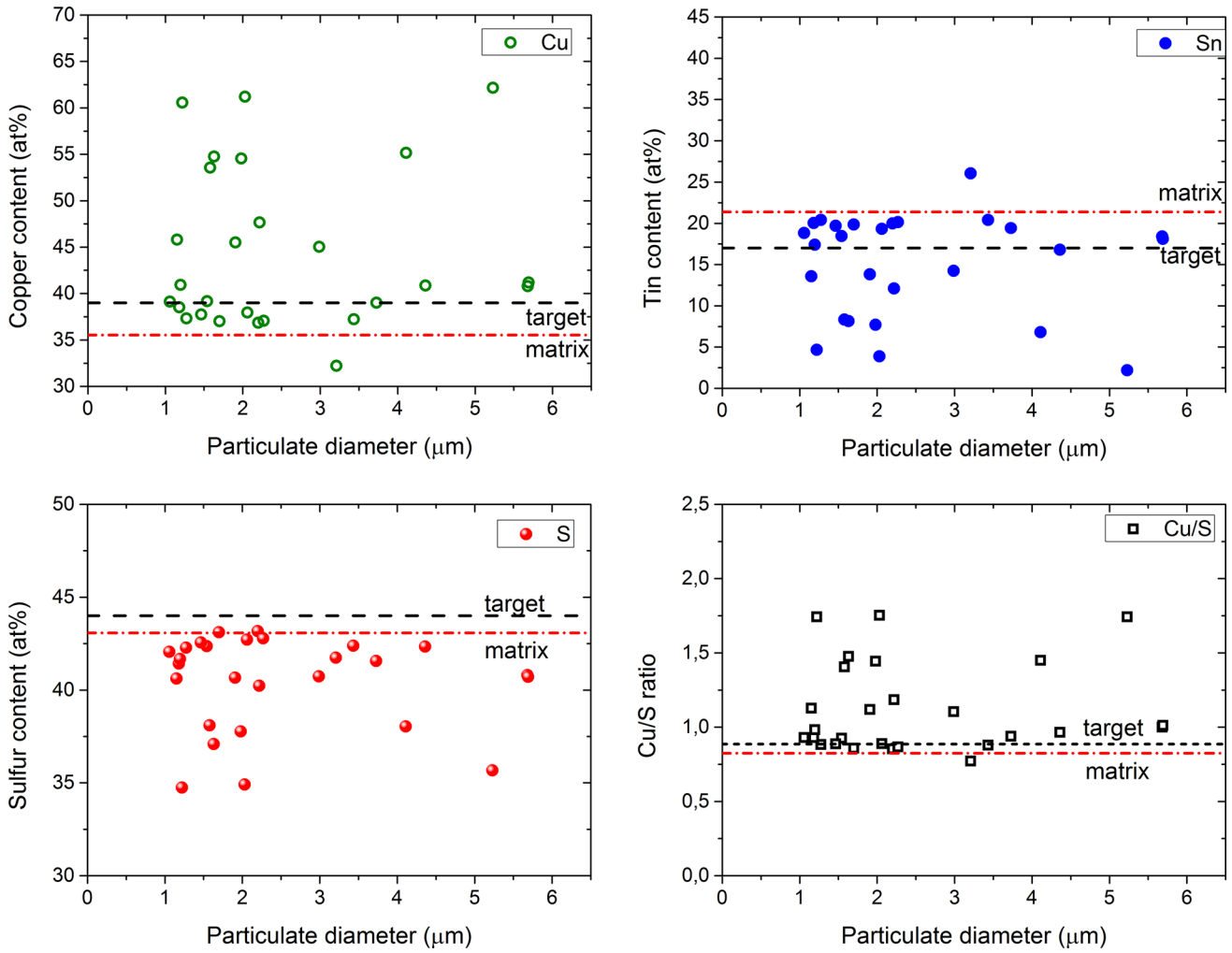

Fig. 5 Compositional analysis of the droplets as a function of droplet diameter for a film made from the non-SnS-enriched CTS target at 1.6 J/cm^2 at 248 nm (note that this target was Cu-rich and S-poor relative to the ideal composition as measured by our EDX analysis; see also Table 2). The Cu, Sn, S content, as well as the Cu/S ratio are given for a random selection of droplets with an average diameter larger than 1 μm. The composition of the target is indicated as "target", while the composition of the underlying film is indicated by "matrix"

between congruent material transfer and the amount of droplets on the films depending on fluence was previously mentioned in the literature, e.g., by Lowndes [11].

An incongruent transfer at low fluence has been observed for other materials (e.g., $SrTiO_3$ [32, 33] and YBCO [34]), and different explanatory models have been offered [11, 33, 34]. Venkatesan et al. [34] pointed out that the non-stoichiometric transfer of the material in the low-fluence regime is correlated with preferential evaporation of the elements with high vapor pressure and low cohesive energy in the multicomponent target. In the case of CTS, Cu has a higher cohesive energy (3.5 eV/atom) than Sn (3.12 eV/atom) (Table 3) [35]. While the cohesive energy of atoms in alloys has only been investigated by a few groups, alloyed atoms nevertheless show a cohesive energy similar to the pure elements [10]. Therefore, it may be expected that in the evaporative regime, the CTS films are Cu-deficient, as seen in the low-fluence films, as this is the least volatile element and thus the most difficult one to ablate.

In the high-fluence regime, ablation results in a distribution of droplets of the order of micrometer size embedded in the CTS films, independent on the irradiation wavelength. In this regime, the transfer of the ablated material is nearly stoichiometric. The films deposited at 355 nm are slightly Cu- and Sn-rich, while the films deposited at 248 nm are slightly Cu-poor. The lower Cu content of the 248-nm films may be linked to the lower intensity of the 248-nm laser pulses, since this would lead to a higher evaporative component for a given fluence. Interestingly, Kautek et al. [18] saw a similar trend in YBCO films made at 266 and 355 nm: The element transfer was incongruent at somewhat higher fluence at 266 nm than at 355 nm, even though in their experiment, both lasers had the same pulse length.

Our observation of a transition from a Cu-poor to a Cu-rich regime with increasing fluence with the 355-nm laser is similar to the transition from Sr-rich to Ti-rich $SrTiO_3$ seen by Ohnishi et al. [32] with increasing fluence. For the deposition of a bimetallic material in an oxygen background gas, it was possible for Onishi et al. to identify a fluence that perfectly balanced the Sr:Ti ratio. In contrast, for the tri-component chalcogenide CTS, it may be that no fluence exists that ensures perfectly stoichiometric transfer. However, we see that it is possible tune the ratio of Sn to Cu by fluence adjustment and to compensate for any S deficiency using a post-deposition sulfurization step, as performed for CZTS films by Moriya et al. [20].

Table 3 Cohesive energy and temperature at which the vapor pressure is 1 Pa for the constituent elements of CTS as well as SnS and Cu_2SnS_3

	Cohesive energy (eV/atom) [35]	Temperature at which the vapor pressure is 1 Pa (°C)
Cu	3.5	963 [31]
Sn	3.12	951 [31]
S	2.86	102 [31]
SnS	NA	590 [38, 39]
Cu_2SnS_3	NA	higher than SnS [30]

Detailed characterization of the droplets embedded in the CTS film deposited at 1.6 J/cm^2 at 248 nm reveals a large depletion in S and Sn relative to Cu in the droplets. The degree of depletion increases with decreasing droplet size. Sulaiman et al. [13] have observed that both Cu- and Sn-rich droplets were transferred onto films of CZTS made by PLD at 355 nm without a detailed qualitative analysis. Chen and Hall [14] have shown that in binary metallic systems of Nb–Al and Nb–Cr, the droplets are usually deficient in the element with high vapor pressure and the deficiency of the volatile elements increases with decreasing droplet size. In the Cu–Sn–S system, the vapor pressure of Cu and Sn is much lower than that of S (see Table 3). As a result, preferential evaporation of S is likely and would result in Cu- and Sn-rich droplets. However, the EDX analysis indicates a deficiency of Sn in the solidified molten droplets in addition to an S deficiency. Since SnS is far more volatile than Sn (Table 3), it is likely that the Sn deficiency is caused by the evaporation of SnS, as proposed by Weber et al. [30] in an investigation of Sn loss from heated films of CZTS.

We do not see a droplet reduction with a change between the two UV laser wavelengths 355 and 248 nm. As described in the introduction, droplet reduction might have been expected if the target absorption of the 248-nm laser was higher than the 355-nm laser so that subsurface boiling would be reduced, or if the 248 nm light was able to more efficiently break up the ejected droplets. As discussed in Sect. 3.1, the absorption of different UV wavelengths in the target is not easily predicted, and the increased photon energy at 248 nm may be offset by the longer pulse length, leading to a lower pulse power. The combined effect of the differences between the lasers in wavelength and pulse length seems to have little influence on this particular material.

For the fabrication of the thin-film absorber layers of CTS for thin-film solar cells, it is desirable to have Cu-poor films [36] and a uniform composition. Since the composition of the droplets can be different to the underlying film, it is important to minimize their occurrence. We observe that splashing and associated Cu-rich droplets can be minimized by reducing the fluence, although the droplet reduction has to be balanced against the appropriate composition. Additional strategies to reduce droplets are to use off-axis deposition, a mechanical velocity filter, or a voltage across the ablation plume [11, 19]. However, these

methods mean that the deposition process becomes far more complex.

5 Conclusion

We have reported on the fabrication of copper tin sulfide (CTS) and SnS-rich CTS thin films in vacuum for two UV wavelengths, 355 and 248 nm. The deposition rate was about four times higher at 355 nm than at 248 nm for both CTS and SnS-rich CTS. The morphology studies of the as-deposited films showed that the area density of the droplets was not reduced by increasing the photon energy from 355 to 248 nm.

For both lasers, the laser fluence significantly affects the density and average size of the droplets. At high fluence (1.6 J/cm^2), UV irradiation leads to near-congruent transfer of the ablated material. Droplets produced by the 248-nm KrF-excimer laser ablation at high fluence were mainly S- and Sn-poor, and the deficiency seemed more pronounced with decreasing droplet size. A reduction in the laser fluence down to 0.2 J/cm^2 resulted in smaller droplets and lower droplet area density for both lasers.

The low-fluence regime leads to incongruent evaporation of films with typically large copper deficiency and therefore films that were S- and Sn-rich relative to the target. The Cu deficiency was most pronounced for the 248-nm laser, possibly due to the lower intensity of the 248-nm laser pulses.

Films deposited by either laser from the SnS-rich CTS target were Sn-rich relative to the desired composition for solar cell absorber layers. Films deposited from the CTS target at 1.6 J/cm^2 by either laser were somewhat Cu-rich for solar cells (we found Cu/Sn $\sim$ 2.0 compared to Cu/Sn $\sim$ 1.7–1.9 in successful solar cells [36, 37]). However, by reducing the fluence somewhat, it will be possible to reach the optimal Cu/Sn ratio with both the 248- and the 355-nm laser.

Overall, our study illustrates the commonly observed trade-off in PLD between reduction in the droplet density and change in the composition with a reduction in the laser fluence.

Acknowledgments This work has been supported by a grant from the Danish Council for Strategic Research.

References

1. D.B. Mitzi, O. Gunawan, T.K. Todorov, D.A.R. Barkhouse, Philos. Trans. R. Soc. A **371**, 20110432 (2013)
2. S. Tajima, T. Itoh, H. Hazama, K. Ohishi, R. Asahi, Appl. Phys. Express **8**, 082302 (2015)
3. T.A. Kuku, O.A. Fakolujo, Sol. Energy Mater. **16**, 199 (1987)
4. P.A. Fernandes, P.M.P. Salomé, A.F. da Cunha, Phys. Status Solidi C **7**(3–4), 901 (2010)
5. P. Zawadzki, L.L. Baranowski, H. Peng, E.S. Toberer, D.S. Ginley, W. Tumas, A. Zakutayev, S. Lany, Appl. Phys. Lett. **103**, 253902 (2013)
6. N. Aihara, H. Araki, A. Takeuchi, K. Jimbo, H. Katagiri, Phys. Status Solidi C **10**, 1086 (2013)
7. M. Nakashima, J. Fujimoto, T. Yamaguchi, M. Izaki, Appl. Phys. Express **8**, 042303 (2015)
8. R.B. Ettlinger, A. Cazzaniga, S. Canulescu, N. Pryds, J. Schou, Appl. Surf. Sci. **336**, 385 (2015)
9. S.A. Vanalakar, G.L. Agawane, A.S. Kamble, C.W. Hong, P.S. Patil, J.H. Kim, Sol. Energy Mater. Sol. Cells **138**, 1 (2015)
10. J. Schou, Appl. Surf. Sci. **255**, 5191 (2009)
11. D.H. Lowndes, in *Laser Ablation Desorption, Experimental Methods in the Physical Sciences*, vol. 30, ed. by J.C. Miller, R.F. Haglund (Academic Press, New York, 1998), pp. 475–571
12. K. Ito, in *Copper Zinc Tin Sulfide-Based Thin Film Solar Cells*, 1st edn., ed. by K. Ito (Wiley, Chichester, West Sussex, 2015), pp. 34–35
13. N.S. Che Sulaiman, C.H. Nee, S.L. Yap, Y.S. Lee, T.Y. Tou, S.S. Yap, Appl. Surf. Sci. **354**, 42 (2015)
14. L.-C. Chen, E.L. Hall, Mater. Res. Soc. Symp. Proc. **285**, 519 (1993)
15. W.O. Siew, S.S. Yap, C. Ladam, Ø. Dahl, T.W. Reenaas, T.Y. Tou, Appl. Phys. A **104**, 877 (2011)
16. N.J. Ianno, L. McConville, N. Shaikh, S. Pittal, P.G. Snyder, Thin Solid Films **220**, 92 (1992)
17. G. Koren, A. Gupta, R.J. Baseman, M.I. Lutwyche, R.B. Laibowitz, Appl. Phys. Lett. **55**, 2450 (1989)
18. W. Kautek, B. Roas, L. Schultz, Thin Solid Films **191**, 317 (1990)
19. L.-C. Chen, in *Pulsed Laser Deposition. Thin Film*, 1st edn., ed. by D.B. Crisey, G.K. Hubler (Wiley, New York, 1994), pp. 167–198
20. K. Moriya, K. Tanaka, H. Uchiki, Jpn. J. Appl. Phys. **47**, 602 (2008)
21. S.M. Pawar, A.V. Moholkar, I.K. Kim, S.W. Shin, J.H. Moon, J.I. Rhee, J.H. Kim, Curr. Appl. Phys. **10**, 565 (2010)
22. K. Ujimoto, T. Yoshimura, A. Ashida, N. Fujimura, Jpn. J. Appl. Phys. **52**, 045803 (2013)
23. D. Drouin, A.R. Couture, D. Joly, X. Tastet, V. Aimez, R. Gauvin, Scanning **29**, 92 (2007)
24. L.I. Berger, in *CRC Handbook of Chemistry and Physics*, 96th edn., ed. by W.M. Haynes, T.J. Bruno, D.R. Lide (CRC Press, Boca Raton, 2015), pp. 12-80–12-93
25. W.M. Haynes, T.J. Bruno, D.R. Lide (eds.), *CRC Handbook of Chemistry and Physics*, 96th edn. (CRC Press, Boca Raton, 2015), pp. 4–43–4–101
26. L.A. Burton, D. Colombara, R.D. Abellon, F.C. Grozema, L.M. Peter, T.J. Savenije, G. Dennler, A. Walsh, Chem. Mater. **25**, 4908–4916 (2013)
27. O. Madelung, U. Rössler, M. Schulz (eds), *Springer Materials Series Landolt-Börnstein - Gr. III Condensed Matter, Subvolume 41C, Non-tetrahedrally Bonded Elements and Binary Compounds I* (Springer, Berlin, 1998), pp. 1–2
28. A. Crovetto, R. Chen, B. Ettlinger, A.C. Cazzaniga, J. Schou, O. Hansen, C. Persson (2016) (submitted)
29. O. Madelung, U. Rössler, M. Schulz (eds.), *Non-tetrahedrally Bonded Elements and Binary Compounds I* (Springer, Berlin, 1998), pp. 1–8
30. A. Weber, R. Mainz, H.W. Schock, J. Appl. Phys. **107**, 013516 (2010)
31. W.M. Haynes, T.J. Bruno, D.R. Lide (eds.), *CRC Handbook of Chemistry and Physics*, 96th edn. (CRC Press, Boca Raton, 2015), pp. 6-88–6-116

32. T. Ohnishi, T. Yamamoto, S. Meguro, H. Koinuma, M. Lippmaa, J. Phys. Conf. Ser. **59**, 514 (2007)
33. B. Dam, J.H. Rector, J. Johansson, J. Huijbregtse, D.G. De Groot, J. Appl. Phys. **83**, 3386 (1998)
34. T. Venkatesan, X.D. Wu, A. Inam, J.B. Wachtman, Appl. Phys. Lett. **52**, 1193 (1988)
35. C. Kittel, *Introduction to Solid State Physics*, 3rd edn. (Wiley, New York, 1966) p. 78
36. A. Kanai, K. Toyonaga, K. Chino, H. Katagiri, H. Araki, Jpn. J. Appl. Phys. **54**, 08KC06 (2015)
37. M. Nakashima, T. Yamaguchi, H. Itani, J. Sasano, M. Izaki, Phys. Status Solidi C **12**, 761 (2015)
38. B. Richards, Trans. Faraday Soc. **51**, 1193 (1955)
39. V. Piacente, S. Foglia, P. Scardala, J. Alloys Compd. **177**, 17 (1991)